Computation of the temperature distortion in the stack of a standing-wave thermoacoustic refrigerator

David Marx and Philippe Blanc-Benon
Centre Acoustique, LMFA, UMR CNRS 5509, Ecole Centrale de Lyon, 36 avenue Guy de Collongues, 69134 Ecully cedex, France

(Received 21 February 2005; revised 1 August 2005; accepted 19 August 2005)

The numerical computation of the flow and heat transfer in the vicinity of a stack plate in a standing wave refrigerator is performed. Temperature distortion is observed, which appears only in the stack region, even if the acoustic standing wave outside the stack is itself sinusoidal. The distortion takes place above the whole plate surface when the length of the plate is equal to or shorter than four times the particle displacement. This condition may occur at high drive ratios and is favored by plate positions close to the velocity antinode. The thermal distortion decreases the thermoacoustic heat pumping along the plate. At high drive ratios, if the length of the plate is not large enough, the thermal distortion can typically explain a difference of about 10% between the calculated heat flux and the heat flux predicted using linear theory. © *2005 Acoustical Society of America.*
[DOI: 10.1121/1.2063087]

PACS number(s): 43.35.Ud, 43.25.−x [RR] Pages: 2993–2999

I. INTRODUCTION

To design and predict the performance of thermoacoustic devices, the most widely used tool is the standard "linear theory."[1] Although very advanced, this theory does not take into account some phenomena such as nonlinear effects, including complex flows. Complex flows include turbulence and motions resulting from abrupt changes of section. Vortical motions at the extremities of the stack plates and heat exchangers have been observed both experimentally and numerically.[2] They can generate minor losses[3–5] that are detrimental to performance. Acoustic nonlinear effects consist of acoustic streaming[6–8] and harmonics generation. In some cases acoustic streaming has been identified and successfully suppressed.[3] The most obvious reason for harmonics generation is the nonlinear propagation of a high-amplitude wave in the resonator.[9–12] Using an appropriate shape for the resonator[13] (or more simply inserts at the harmonics velocity antinode) these harmonics can be removed. From a different nature are the thermal harmonics resulting from the thermal interaction between the stack and the oscillating gas, which were theoretically predicted by use of an inviscid nonlinear model.[14] Some results previously reported by the authors confirmed the distortion of the temperature oscillation at high acoustic amplitudes in the stack region.[15]

All together, nonlinear phenomena have a very important effect on thermoacoustic device performance, and their knowledge is especially important to predict the saturation amplitude of thermoacoustic engines. The parameter used in thermoacoustics to describe the amplitude of the wave is the drive ratio, defined as the ratio of the acoustic pressure amplitude at the pressure antinode to the mean pressure in the resonator. For standing wave devices, nonlinear effects are generally considered to appear when the drive ratio is more than about 2% or 3%.[16,17] Though this limit is somewhat arbitrary since it depends on the configuration of the system and on the type of nonlinearity that happens to be the critical one in the system. Nevertheless, for practical drive ratios of 10%, a typical 10% error on the heat flux is observed in standing-wave devices, even in precisely controlled experiments.[10,18] Results reported here may explain part of the difference between theoretical predictions and experimental results. In the paper we deal with the computation of nonlinear temperature effects in a standing wave thermoacoustic refrigerator. In Sec. II the numerical modeling of the problem is briefly explained. Results of the simulations are then presented in Sec. III. They concern mainly the distortion of the time variation of the temperature in the stack region. A discussion is made in Sec. IV, where results are interpreted using the previous analysis by Gusev *et al.*[14] Some implications of the temperature distortion on the thermoacoustic heat pumping are also given. The main conclusions are drawn in Sec. IV.

II. METHODS

To include most of the physical phenomena involved in thermoacoustic heat pumping (boundary layers, nonlinear acoustics, heat transfer, temperature gradient, two-dimensional flow), a numerical solver has been developed.[15,19] It is based on the solution of the two-dimensional compressible and unsteady Navier–Stokes equations, coupled with mass and energy conservation equations. The governing equations for a perfect gas are

$$p = \rho r T, \tag{1}$$

$$\frac{\partial \rho}{\partial t} + \nabla \cdot (\rho \mathbf{u}) = 0, \tag{2}$$

$$\frac{\partial (\rho \mathbf{u})}{\partial t} + \nabla \cdot (\rho \mathbf{u}\mathbf{u}) + \nabla p = \nabla \cdot \boldsymbol{\tau}, \tag{3}$$

$$\frac{\partial T}{\partial t} + \mathbf{u}\cdot\boldsymbol{\nabla} T + (\gamma - 1) T \boldsymbol{\nabla}\cdot\mathbf{u} = \frac{(\gamma - 1)}{\rho r}[\Phi + \boldsymbol{\nabla}\cdot(K\,\boldsymbol{\nabla} T)], \tag{4}$$

where the components of the viscous stress tensor $\boldsymbol{\tau}$ are

$$\tau_{xx} = \frac{4}{3}\mu\frac{\partial u}{\partial x} - \frac{2}{3}\mu\frac{\partial v}{\partial y},$$

$$\tau_{xy} = \tau_{yx} = \mu\left(\frac{\partial u}{\partial y} + \frac{\partial v}{\partial x}\right), \tag{5}$$

$$\tau_{yy} = \frac{4}{3}\mu\frac{\partial v}{\partial y} - \frac{2}{3}\mu\frac{\partial u}{\partial x},$$

and the viscous dissipation, Φ, is defined by

$$\Phi = 2\mu\left[\left(\frac{\partial u}{\partial x}\right)^2 + \left(\frac{\partial v}{\partial y}\right)^2 + \frac{1}{2}\left(\frac{\partial u}{\partial y} + \frac{\partial v}{\partial x}\right)^2 - \frac{1}{3}\left(\frac{\partial u}{\partial x} + \frac{\partial v}{\partial y}\right)^2\right]. \tag{6}$$

In these expressions T is the temperature, p is the pressure, ρ is the density, $\mathbf{u}=[u;v]$ is the velocity vector; r is the gas constant, γ is the ratio of specific heats, μ is the shear viscosity, and K is the thermal conductivity. The temperature dependence of μ and K is not taken into account, which is a reasonable approximation because the temperature gradients are small in the present case. For air, $\mu = 1.8\times10^{-5}$ Pa s; $K = 2.5\times10^{-2}$ W K^{-1} m^{-1}; $r = 287$ J K^{-1} kg^{-1}; $\gamma = 1.4$. Equations (1)–(4) are used to solve for the variables p, ρ, $\mathbf{u}$, and T. The calculation is started from a initial state consisting of ambient values for the thermodynamic variables and zero velocity, and is performed until the rate of growth becomes negligible. To solve Eqs. (1)–(4), fourth-order dispersion-relation-preserving finite differences are used for calculating spatial derivatives, and time integration is performed using a four-step Runge–Kutta method. Dispersion-relation-preserving methods are used to minimize the error between physical and numerical dispersion relations.[20] These accurate methods are chosen to calculate second-order quantities (thermoacoustic heat pumping, mass streaming, and potentially minor losses[5]) superimposed on a first-order acoustic field. As they introduce little dissipation, spurious waves can appear and are filtered using high-order filters.[21] The solver allows the simulation of the flow and heat transfer in the vicinity of a stack plate in the presence of an acoustic standing wave. The plate may be either of negligible or finite thickness, and be either heat conducting or isothermal. The more complex are the geometry and the thermal model, the more important the computational cost will be. It can sometimes be prohibitive. In the present paper we will focus on the case of an isothermal plate of negligible thickness. The effect of the plate is to impose a fixed temperature (as well as a no-slip) condition on its surface, so that no additional energy conservation equation needs to be solved for the plate. The isothermal plate model has already been used in some other numerical simulations, mostly for its simplicity.[22,23] It should be noticed that despite this model prevents one from getting a temperature gradient in the plate itself, it allows a temperature gradient to establish within the fluid above the plate. This gradient if somewhat reduced because of the isothermal condition, but this indeed tends to increase the thermoacoustic heat pumping along the plate. It turns out that the use of an isothermal boundary condition does not modify the validity of the results presented below, as will be mentioned below.

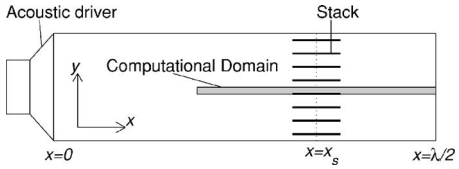

FIG. 1. Sketch of the thermoacoustic refrigerator.

The thermoacoustic refrigerator is represented in Fig. 1, where the grayed-out area is the computational domain. The abscissa origin is taken at the acoustic driver. The length of the resonator is half the wavelength, λ. The position of the stack middle point is x_s. The computational domain is shown in Fig. 2. The computational domain takes advantage of the periodic nature of the stack and includes only one plate of the stack. Symmetric boundary conditions are used on the lateral boundaries of the domain, an approach that has been used in all thermoacoustic simulations[22–24] in order to decrease the computational time. The acoustic standing wave that is required in a standing wave refrigerator is created in a physical way: by superimposing two counterpropagating traveling waves. More precisely, a traveling wave is continuously injected into the domain through the S_{wave} boundary. This wave travels up to the rigid end, where it is reflected. There is thus also a reflected traveling wave that travels from the rigid end toward the surface S_{wave}, where it goes out of the domain. The S_{wave} surface has a double role: to inject the direct right-traveling wave and to let escape the reflected left-traveling wave. Numerically this is done using the method of characteristics.[25] The superimposition of the direct and reflected traveling waves creates a standing wave. The total distance covered by the traveling wave (first direct and then reflected) during its stay in the domain is twice the length of the domain; this is less than a wavelength. As a consequence, the wave has not enough time to be modified by nonlinear effects during its propagation, even at the high

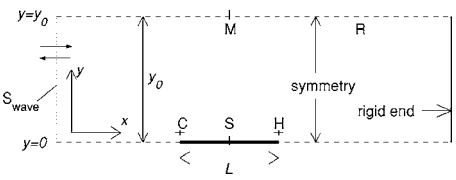

FIG. 2. Sketch of the computational domain. Point S is in the middle of the plate. Point C is in the fluid just above the plate extremity, in the cold region. Point H is in the fluid just above the other extremity, in the hot region.

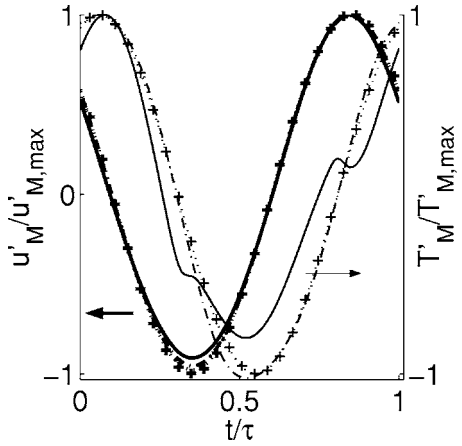

FIG. 3. Time variation of the temperature at point M, T'_M, divided by the maximum value of this variation, $T'_{M,\max}$, and time variation of the velocity at point M, u'_M, divided by the maximum value of this variation, $u'_{M,\max}$. The values for the drive ratio are $+++$, $D_r=0.7\%$; $\cdots$, $D_r=2.8\%$; $---$, $D_r=5.6\%$; —, $D_r=11.2\%$. Thin symbols are for temperature; bold symbols are for velocity.

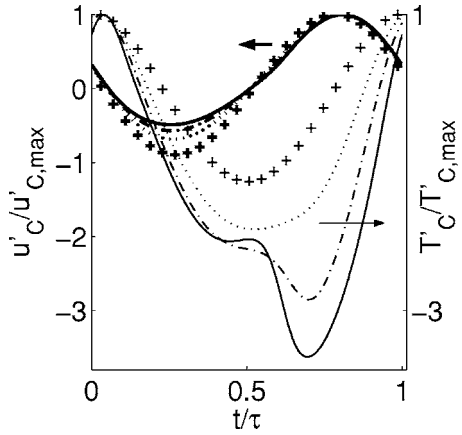

FIG. 4. Time variation of the temperature at point C, T'_C, divided by the maximum value of this variation, $T'_{C,\max}$, and time variation of the velocity at point C, u'_C, divided by the maximum value of this variation, $u'_{C,\max}$. The values for the drive ratio are $+++$, $D_r=0.7\%$; $\cdots$, $D_r=2.8\%$; $---$, $D_r=5.6\%$; —, $D_r=11.2\%$. Thin symbols are for temperature; bold symbols are for velocity.

amplitudes that will be considered in the following. This allows to get a high-amplitude standing wave with nearly no harmonics.

III. RESULTS

In the following, any quantity, ψ, will be written $\psi=\psi_0+\psi'$, where the subscript 0 indicates a quantity at rest, and the prime indicates the perturbation of that quantity when there is an acoustic wave in the domain. Hence, ψ' includes the first-order perturbation (ψ_1) as well as all the terms of higher order, including harmonics and time-averaged terms. With these notations, the drive ratio is $D_r=p'(\lambda/2)/p_0$. This is the ratio of the acoustic pressure at the rigid end of the resonator (located at $x=\lambda/2$; see Fig. 1) to the pressure p_0 when the system is at rest. The density, temperature, and pressure at rest are $\rho_0=1.2\ \mathrm{kg\ m^{-3}}$, $T_0=298$ K, and $p_0=100$ kPa, respectively. The velocity at rest is simply $u_0=0$. The speed of sound is $c_0=\sqrt{\gamma r T_0}$. Important quantities in thermoacoustic are the viscous and thermal penetration depth defined, respectively, by $\delta_\nu=\sqrt{\mu/\rho_0\pi f}$ and $\delta_\kappa=\sqrt{K/\rho_0 c_p \pi f}$, where $c_p=\gamma r(\gamma-1)$ is the isobaric specific heat, and f is the frequency. The height, y_0, of the computational domain is such that $y_0/\delta_\kappa=2.5$, a typical value for thermoacoustic stacks. The mesh size is equal to $\delta_\kappa/7.3$ (except for Fig. 6, later, where it is $\delta_\kappa/10$), a value that has proved sufficient for these simple calculations.[19] The plate length, L is such that $L=\lambda/40$. The position of the plate will be expressed in the normalized form kx_s, where $k=2\pi/\lambda$ is the wave number. This position will be fixed at $kx_s=2.13$, except in Fig. 6 (later)

As a nonlinear behavior generally implies some distortion, the time variations of the velocity and temperature were recorded at several points of the computational domain. The temperature time variation at point M of the domain (see Fig. 2) is shown in Fig. 3 for different values of the drive ratio. Temperature T'_M is made dimensionless using its maximal value during the acoustic cycle $T'_{M,\max}$. Time is made dimensionless using the acoustic period, τ. At lower drive ratios, $D_r=0.7\%$ and $D_r=2.8\%$, the temperature variation is sinusoidal. For a higher drive ratio, $D_r=5.6\%$, the temperature time variation slightly departs from a sinusoidal curve. For the higher drive ratio represented, $D_r=11.2\%$, the temperature variation is clearly distorted, showing the importance of nonlinear effects. The computed variations of the temperature are periodic of the acoustic period τ; thus the temperature distortion is made of harmonics of the fundamental. This was also verified using a Fast Fourier Transform. Hence, in the following, *temperature distortion* and *temperature harmonics generation* will have the same meaning. In all the cases considered in this paper, the FFT showed also that only five or six harmonics had a non-negligible amplitude, with the first and second having a major contribution. The time variation of the velocity at point M for different drive ratios is also shown in Fig. 3. As can be seen, the velocity time variation, unlike the temperature variation, remains sinusoidal, even for the highest value of the drive ratio, $D_r=11.2\%$. The normalized velocity is indeed slightly modified in its most negative values when the drive ratio increases, in such a way that the time-averaged velocity at point M over one acoustic cycle becomes slightly positive. This is consistent with observation of acoustic streaming above the plate[26] (here the nonzero mean velocity is due to "inner" vortices[8]). Nevertheless, this effect remains small.

The temperature time variation was also recorded at point C of the domain (see Fig. 2), located in the fluid, just above the extremity of the plate, in the cold region (the stack is pumping heat from cold point C to hot point H). This variation is shown in Fig. 4 for different values of the drive ratio. Even for the lower drive ratios, $D_r<5.6\%$, the temperature variation is not sinusoidal. At the highest drive ratio, $D_r=11.2\%$, the nonsinusoidal behavior of the temperature at point C is much more pronounced than that at point M at the same drive ratio. Velocity variation at point C is also shown in Fig. 4. Again, unlike the temperature variation, the velocity variation at point C remains sinusoidal for the whole range of the drive ratio. It is almost obvious from Fig. 4 that the time-averaged temperature and velocity over one acous-

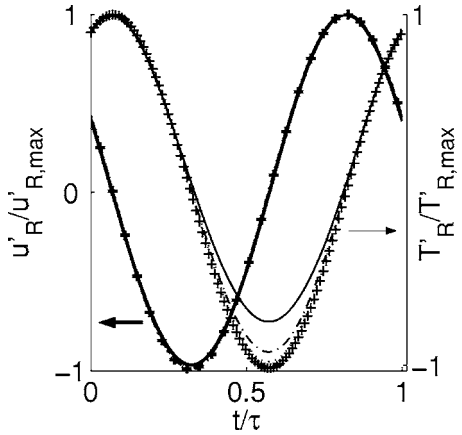

FIG. 5. Time variation of the temperature at point R, T'_R, divided by the maximum value of this variation, $T'_{R,\max}$, and time variation of the velocity at point R, u'_R, divided by the maximum value of this variation, $u'_{R,\max}$. The values for the drive ratio are $+++$, $D_r=0.7\%$; $\cdots$, $D_r=2.8\%$; $---$, $D_r=5.6\%$; —, $D_r=11.2\%$. Thin symbols are for temperature; bold symbols are for velocity.

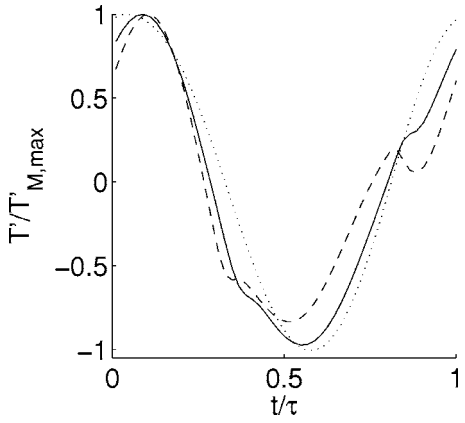

FIG. 6. Temperature time variation at point M, T'_M, divided by its maximum value, $T'_{M,\max}$, for several positions of the plate in the domain: ---, $kx_s=2.07$; —, $kx_s=2.35$; $\cdots$, $kx_s=2.81$. For all three curves, $D_r=11.2\%$.

tic cycle are not zero. The mean value of the temperature is logically negative, since point C is located in a cold region. The nonzero value of the time-averaged velocity comes from time-averaged motions at the end of the plate.[26] These mean motions can roughly be explained as follows. First note that the fluid in, say, the viscous boundary layer above the plate, is almost at rest. This means that although the plate itself has a negligible thickness, the plate plus the fluid at rest just above it may be considered as a plate of nonzero thickness. Thus, the flow of the fluid located outside the viscous layer sees a "step" at the junction between the resonator and the plate. At point C, during the half of the acoustic period when the fluid moves leftward there is a decreasing step, with the creation of anticlockwise vortices. During the half of the acoustic period when the fluid moves rightward, there is a raising step, which creates much less vorticity. On average, there is a mean anticlockwise vortical flow at the end of the plate at point C, which explains why the mean velocity at this point is not zero.

The temperature and velocity variations at point R of the domain are given in Fig. 5 for different values of the drive ratios. Point R is located in the core of the resonator, at an equal distance from the plate and the end wall. At this location both temperature and velocity variations remain sinusoidal, unlike what happens at point M or point C. This also confirms that the method used to sustain the wave in the resonator creates a high drive ratio standing wave without any wave steepening. Note that the mean temperature at point R is positive, since point R is located in the hot part of the resonator located between the stack and the rigid end.

It was stated in a previous study[15] that the temperature distortion tend to disappear when the plate is moved toward the velocity node, which is toward the rigid end of the resonator. This is indeed shown in Fig. 6. In this figure, the time variation of the temperature at point M is plotted for different values of the normalized position kx_s, at a drive ratio $D_r=11.2\%$. For a position close to the velocity antinode, $kx_s=2.07$, temperature harmonics are visible. They disappear when the plate is located at $kx_s=2.81$, closer to the velocity node.

IV. DISCUSSION

The results given above show that in the stack region (points C and M) the temperature may be nonsinusoidal, while the velocity remains harmonic. Far from the stack region (point R), the temperature and velocity both remain sinusoidal, even at high drive ratios. It means that temperature harmonics creation is taking place in the stack only. Moreover this creation is more effective at the extremities of the stack plates, since harmonics, when present at both points M and C, are stronger at point C. It also means that in the stack region, the nonlinear term of the momentum equation $(u\cdot\nabla u)$ has a much less important effect than the corresponding term in the energy equation $(u\cdot\nabla T)$. This is partly taken into account in the linear theory, since in the linearization the term $(u\cdot\nabla u)$ disappears, while the term $(u\cdot\nabla T)$ is kept and replaced by $(u\cdot\nabla T_m)$, where T_m is the mean temperature. But even if they take into account the effect of mean temperature variation, the linearized equations cannot account for the temperature harmonics observed above.

The results presented above can be explained by considering the analysis made by Gusev *et al.*[14] Using an inviscid but nonlinear model (the term $u\cdot\nabla T$ is fully preserved in their energy equation), these authors have shown that the nonlinear convective term $u\cdot\nabla T$ in the energy equation is responsible for temperature harmonics generation at the edges of the plate. This generation exists because of the energy exchange between the plate and the fluid at that location.[22] This exchange itself occurs because of the thermoacoustic heat flux entering or leaving the plate at its extremities. The point at which the temperature harmonics generation occurs are located within two particle displacements from the extremities of the stack. Moreover, harmonics generation is more important closer to the extremity of the plate. In Fig. 7(a), the grayed-out regions at each extremity of the plate represent regions in which there is harmonics generation. The height of these regions are simply of the order of the thermal penetration depth (that is of the order of y_0),

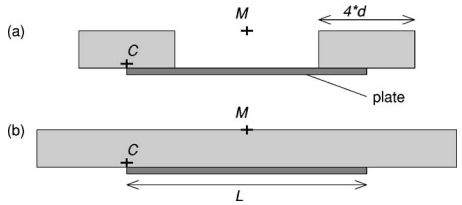

FIG. 7. In a grayed-out area, the temperature variation has a nonlinear behavior, that is, harmonics are created. Two cases are represented: (a) The acoustic displacement amplitude, d, is small compared with the plate length, L; (b) the particle displacement amplitude, d, is of the order of L.

since it is the characteristic length for heat transfer between the fluid and the plate. Their length is four times the particle displacement, d, defined by

$$d = \frac{u'}{2\pi f}. \tag{7}$$

For a standing wave in the resonator, the particle displacement at the stack position is

$$d = \gamma D_r \frac{\lambda}{2\pi} \sin(kx_s). \tag{8}$$

Importantly, the particle displacement increases with the drive ratio, and depends on the position x_s of the stack. In their analysis, Gusev *et al.* comment the case when the particle displacement is small compared with the plate length. This happens at low drive ratios. This case is represented in Fig. 7(a). In particular, in this figure point C belongs to the grayed-out region, but not point M. This explains why at low drive ratios, temperature harmonics are observed at point C (Fig. 4) but not at point M (Fig. 3). When the drive ratio increases, the particle displacement increases as well, and the situation may correspond to the sketch of Fig. 7(b). In this figure, both points C and M belong to the grayed-out region, which explains why at high drive ratios, temperature harmonics are observed at both locations (Fig. 3 and Fig. 4). Actually, the nonlinear region extends gradually when the drive ratio increases, and is expected to reach point M and cover the whole plate when the drive ratio is such that $L = 4d$, that is when

$$L = 4\gamma D_r \frac{\lambda}{2\pi} \sin(kx_s). \tag{9}$$

This equation defines a critical length for the stack, and is expected from the analysis. It is obtained using Eq. (8), which does not take into account the presence of the plate. It has indeed been observed in the computations that the temperature nonlinearities are observed at point M when $L \sim 4d_M$, where d_M is the actual (computed) value of the particle displacement at point M. Considering the critical length defined by Eq. (9), whether the temperature variation above the plate is nonsinusoidal is expected to depend on two parameters: the drive ratio and the position of the plate. The dependence on the drive ratio has just been explained. The effect of plate position was demonstrated in Fig. 6: at a fixed drive ratio, harmonics may appear if the plate is close to the velocity antinode (small kx_s), but not if the plate is moved toward the velocity node (large kx_s).

Hence, all the results obtained numerically may be explained using the theory by Gusev *et al.*[14] Let us mention that the analysis of Gusev *et al.* dealt with a nonviscous fluid. In an earlier part of the work and in an attempt to decouple as much as possible the different sources of nonlinearity, inviscid simulations were performed so that only the thermal interaction with the stack was accounted for. In terms of temperature variation the results were very similar to those presented in the present paper, where viscosity is taken into account. It appears that taking into account the viscosity in the present calculations does not prevent the apparition of nonlinear temperature harmonics, nor does it create any velocity harmonic. One consequence of taking viscosity into account is that the velocity is canceled on the plate surface due to no-slip boundary conditions. This effect may be compared to the thermal effect of the plate, which is to cancel the fluid temperature variation on the plate surface (due to isothermal boundary condition, or, more generally, due to the large specific heat of the plate). Despite this similarity, the velocity and temperature have different behaviors. One reason for this is that no momentum is exchanged between the plate and the fluid, while thermal energy is, particularly at the extremities of the plate. One could questions whether the use of an isothermal boundary has an important effect on the thermal harmonics generation. The thermal generation occurs as soon as there is a heat exchange between the plate and the fluid, with large associated temperature gradients. Hence, it is expected to appear with a plate having itself a variable temperature (solved using a solid energy conservation equation). Indeed harmonics generation has been observed for isothermal and nonisothermal plates, of negligible or finite thickness.[19] Petculescu and Wilen[27] conclude from their experiments that the linear theory can be used to describe the thermoacoustic heat pumping along a plate, even when the particle displacement is larger than the plate. Their conclusion is different from the one given in the present paper. But their experimental condition is also very different. In the experiment of Petculescu and Wilen, the plate is embedded within a wall. This wall can thermally interact with the fluid particle when the particle just leaves the plate surface. This is very different from the present configuration, where the fluid that is outside the plate has nothing to interact with and has an adiabatic movement. The present configuration is indeed more representative of a practical stack. Nevertheless it can be inferred that the thermal harmonics generation could possibly be decreased by the presence of heat exchangers, since these exchangers would reduce the heat transfer discontinuity between the fluid and the plate.

One effect often associated with harmonics generation in a signal is the saturation of the amplitude of this signal. The maximal value of the temperature variation at point M, $T'_{M,\max}$, is plotted as a function of the drive ratio in Fig. 8. For low drive ratios, $T'_{M,\max}$ is a linear function of the drive ratio. For a drive ratio of about 5.6%, the temperature maximal value is almost saturating. This corresponds to the appearance of harmonics at point M.

The effect of temperature harmonics creation on heat flux carried along the plate is now discussed. The mean

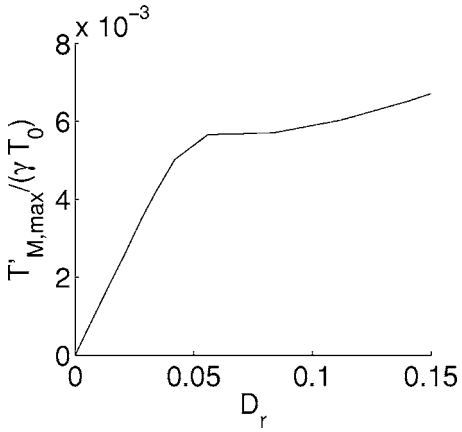

FIG. 8. Effect of the drive ratio, D_r, on the maximum value of the temperature variation at point M, $T'_{M,\max}$.

(time-averaged) thermoacoustic enthalpy flux integrated over the cross section SM of the computational domain is[1]

$$H_{xm}(x_s) = \int_{y=0}^{y=y_0} h_{xm}(x_s, y)dy, \tag{10}$$

where

$$h_{xm}(x,y) = c_p\langle[\rho_0 + \rho'(x,y)]u'(x,y)T'(x,y)\rangle_t, \tag{11}$$

where $\langle\cdot\rangle_t$ is the time average operator. The nonintegrated mean enthalpy flux h_{xm} depends on the vertical position y. The integrated mean enthalpy flux is calculated in section SM located at $x=x_s$ (see Figs. 1 and 2). A term $c_pT_0\langle(\rho_0+\rho')u'\rangle_t$ has been implicitly omitted in Eq. (11) because the section average of this term in Eq. (10) is zero, no net mass flux being possible in a closed-end device. It is also recalled that $u_0=0$. Equation (11) is very well approximated by $h_{xm}=\rho_0 c_p\langle u'T'\rangle_t$, the effect of the density fluctuation being small. Since H_{xm} depends on T', any harmonics generation in T' will have an effect on H_{xm}. In particular, the maximal temperature saturation has a limiting effect on the enthalpy flux. This is shown in Fig. 9, where H_{xm} is plotted as a

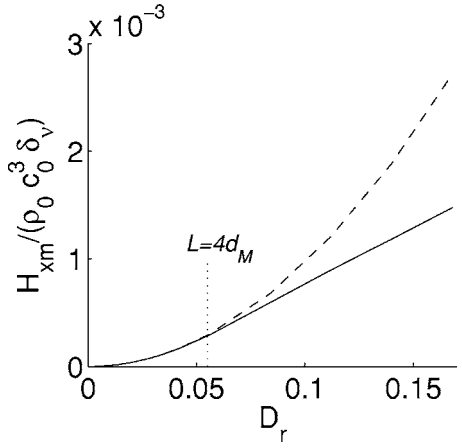

FIG. 9. Section-averaged mean enthalpy flux carried along the plate, H_{xm}, as a function of the drive ratio, D_r: —, calculated flux; ---, D_r^2 fitting at low values of D_r. A vertical dotted line is plotted at $D_r=5.6\%$, which is such that the length of the plate, L, is four times the particle displacement at point M, d_M.

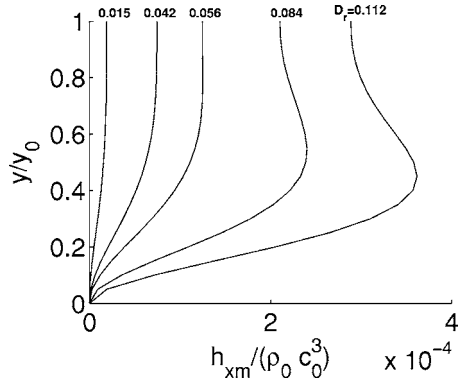

FIG. 10. Spatial variation of mean enthalpy flux, h_{xm}, over the section SM of the computational domain, with the drive ratio as a parameter.

function of the drive ratio. Also plotted in the figure is a fitting at low drive ratios, which dependence is in D_r^2. Such a dependence is being expected from the linear theory. The enthalpy flux matches the fitting curve up to a drive ratio of about 5%, when temperature harmonics appear first at point M. For drive ratios above 5%, H_{xm} depends only linearly on D_r. Given the saturation of the temperature observed in Fig. 8, this linear dependence comes from the velocity term in Eq. (11). In Fig. 9 is also indicated the drive ratio for which the length of the plate, L, is equal to four times the computed particle displacement at point M, d_M.

When a temperature harmonic is created, the thermal boundary layer thickness associated with this harmonic is different from the thermal boundary layer thickness associated with the fundamental (since the thermal boundary layer depends on the frequency). As a result, the temperature waveform above the plate is modified. This also has an effect on the distribution of the enthalpy flux within one cross section above the plate. The spatial variation of $h_{xm}(x_s,y)$ (the mean enthalpy flux within section SM of the computational domain) is shown in Fig. 10 for several values of the drive ratios. The profile of the enthalpy flux is modified for drive ratios above 5.6%. This is because the profile of the temperature itself changes.

Hence, the apparition of thermal harmonics may have an effect on the enthalpy flux carried along the plate. The effect is negligible at low drive ratios when harmonics only appear at the extreme edges of the stack. If the length of the plate is such that the harmonics spread onto the plate at high drive ratios, their effect is to decrease the heat pumping by the plate. The criterion $L=4d_M$ can roughly be used to decide whether it is the case. It has been observed, for example, that this reduction in heat flux decreases the temperature difference between the extremities of a stack plate placed in an acoustic resonator.[28] Typically, harmonics generation may account for a 10% difference between measurements and linear theory predictions. In Fig. 9, at $D_r=0.10$, the difference between the computed curve and the fitting is about 20%, for a plate located close to the velocity antinode where harmonics generation is easily observed.

V. CONCLUSION

The numerical computation of flow and heat transfer in the vicinity of an isothermal plate of negligible thickness

placed in an acoustic standing wave has been performed. A distortion of the temperature oscillation has been observed, and all observations could be explained by referring to a former nonlinear analysis. The temperature harmonics appear only in the stack region, even when the acoustic standing wave itself is sinusoidal and contains no harmonic. They are present above the whole plate surface when the length of the plate is equal to or shorter than four times the particle displacement. This condition may occur at high drive ratios and is favored by plate positions close to the velocity antinode. The thermal harmonics generation decreases thermoacoustic heat pumping by the plate. Fortunately, in standing wave thermoacoustic devices, the optimal position of the stack is closer to the pressure antinode than to the velocity antinode. Nevertheless, at high enough drive ratios, if the length of the plate is not large enough, a difference of about 10% between obtained and predicted heat fluxes can typically occur.

ACKNOWLEDGMENTS

The authors acknowledge the French Ministry of Defense (DGA, Délégation Générale pour l'Armement) for its financial support. Calculations were partially performed using the IDRIS (Institut du Développement et des Ressources en Informatique Scientifique) computing center.

[1]G. W. Swift, "Thermoacoustic engines," J. Acoust. Soc. Am. **84**, 1145–1180 (1988).
[2]Ph. Blanc-Benon, E. Besnoin, and O. Knio, "Experimental and computational visualization of the flow field in a thermoacoustic stack," C. R. Mec. **331**, 17–24 (2003).
[3]S. Backhaus and G. W. Swift, "A thermoacoustic Stirling heat engine: detailed study," J. Acoust. Soc. Am. **107**, 3148–3166 (2000).
[4]R. S. Wakeland and R. M. Keolian, "Influence of velocity profile non uniformity on minor losses for flow exiting thermoacoustic heat exchangers," J. Acoust. Soc. Am. **112**, 1249–1252 (2002).
[5]P. J. Morris, S. Boluriaan, and C. M. Shieh, "Numerical simulation of minor losses due to a sudden contraction and expansion in high amplitude acoustic resonators," Acta. Acust. Acust. **90**, 393–409 (2004).
[6]R. Waxler, "Stationary velocity and pressure gradients in a thermoacoustic stack," J. Acoust. Soc. Am. **109**, 2739–2750 (2001).
[7]H. A. Bailliet, V. Gusev, R. Raspet, and R. A. Hiller, "Acoustic streaming in closed thermoacoustic devices," J. Acoust. Soc. Am. **110**, 1808–1821 (2001).
[8]M. F. Hamilton, Y. A. Ilinskii, and E. A. Zabolotskaya, "Acoustic streaming generated by standing waves in two-dimensional channels of arbitrary width," J. Acoust. Soc. Am. **113**, 153–160 (2003).
[9]A. A. Atchley, H. E. Bass, and T. J. Hofler, "Development of nonlinear waves in a thermoacoustic prime mover," in *Frontiers of Nonlinear Acoustics: 12th ISNA*, edited by M. F. Hamilton and D. T. Blackstock (Elsevier, New York, 1990), pp. 603–608.
[10]G. W. Swift, "Analysis and performance of a large thermoacoustic engine," J. Acoust. Soc. Am. **92**, 1551–1563 (1992).
[11]M. F. Hamilton, Y. A. Ilinskii, and E. A. Zabolotskaya, "Nonlinear two-dimensional model for acoustic engines," J. Acoust. Soc. Am. **111**, 2076–2086 (2002).
[12]S. Karpov and A. Prosperetti, "A nonlinear model of thermoacoustic devices," J. Acoust. Soc. Am. **112**, 1431–1444 (2002).
[13]C. C. Lawrenson, B. Lipkens, T. S. Lucas, D. K. Perkins, and T. W. Van Doren, "Measurements of macrosonic standing waves in oscillating closed cavities," J. Acoust. Soc. Am. **104**, 623–636 (1998).
[14]V. Gusev, P. Lotton, H. Bailliet, S. Job, and M. Bruneau, "Thermal wave harmonics generation in the hydrodynamical heat transport in thermoacoustics," J. Acoust. Soc. Am. **109**, 84–90 (2001).
[15]D. Marx and Ph. Blanc-Benon, "Numerical simulation of stack-heat exchangers coupling in a thermoacoutic refrigerator," AIAA J. **42**, 1338–1347 (2004).
[16]M. E. Poese and S. L. Garrett, "Performance measurements on a thermoacoustic refrigerator driven at high amplitudes," J. Acoust. Soc. Am. **107**, 2480–2486 (2000).
[17]A. A. Atchley, T. J. Hofler, M. L. Muzerall, M. D. Kite, and C. Ao, "Acoustically generated temperature gradients in short plates," J. Acoust. Soc. Am. **88**, 251–263 (1990).
[18]D. L. Gardner and G. W. Swift, "A cascade thermoacoustic engine," J. Acoust. Soc. Am. **114**, 1905–1919 (2003).
[19]D. Marx, "Simulation numérique d'un réfrigérateur thermoacoustique," Ph.D. thesis 2003–34, Ecole Centrale de Lyon, 2003.
[20]C. K. W. Tam and J. C. Webb, "Dispersion-relation-preserving difference schemes for computational aeroacoustics," J. Comput. Phys. **107**, 262–281 (1993).
[21]C. Bogey and C. Bailly, "A family of low dispersive and low dissipative explicit schemes for flow and noise computations," J. Comput. Phys. **194**, 194–214 (2004).
[22]N. Cao, J. R. Olson, G. W. Swift, and S. Chen, "Energy flux density in a thermoacoustic couple," J. Acoust. Soc. Am. **99**, 3456–3464 (1996).
[23]H. Ishikawa and D. J. Mee, "Numerical investigations of flow and energy fields near a thermoacoustic couple," J. Acoust. Soc. Am. **111**, 831–839 (2002).
[24]A. S. Worlikar and O. Knio, "Numerical simulation of a thermoacoustic refrigerator. Part 2: Stratified flow around the stack," J. Comput. Phys. **144**, 299–324 (1998).
[25]K. W. Thompson, "Time dependent boundary conditions for hyperbolic systems," J. Comput. Phys. **68**, 1–24 (1987).
[26]D. Marx and Ph. Blanc-Benon, "Computation of the mean velocity field above a stack plate in a thermoacoustic refrigerator," C. R. Mec. **332**, 867–874 (2004).
[27]G. Petculescu and L. A. Wilen, "High-amplitude thermoacoustic effects in a single pore," J. Acoust. Soc. Am. **109**, 942–948 (2001).
[28]D. Marx and Ph. Blanc-Benon, "Numerical calculation of the temperature difference between the extremities of a thermoacoustic stack plate," Cryogenics **45**, 163–172 (2005).